Physics of the Earth and Planetary Interiors 188 (2011) 114–120

Contents lists available at ScienceDirect

Physics of the Earth and Planetary Interiors

journal homepage: www.elsevier.com/locate/pepi

Melting and thermal pressure of hcp-Fe from the phonon density of states

Caitlin A. Murphy [a,*], Jennifer M. Jackson [a], Wolfgang Sturhahn [b,1], Bin Chen [a]

[a] Seismological Laboratory, California Institute of Technology, M/C 252-21, Pasadena, CA 91125, USA
[b] Advanced Photon Source, Argonne National Laboratory, 9700 S. Cass Avenue, Argonne, IL 60439, USA

ARTICLE INFO

Article history:
Received 18 March 2011
Received in revised form 2 June 2011
Accepted 4 July 2011
Available online 13 July 2011
Edited by Kei Hirose

Keywords:
Earth's core
Nuclear resonant scattering
High pressure
Phonon density of states
Melting of iron
Thermal pressure

ABSTRACT

We directly probed the phonon density of states (DOS) of hexagonal close-packed iron (ε-Fe) with high statistical quality between pressures of 30 GPa and 151 GPa using nuclear resonant inelastic X-ray scattering and *in situ* synchrotron X-ray diffraction experiments at 300 K. From each measured phonon DOS, we determined the vibrational free energy (F_{vib}) and mean-square displacement of atoms, $\langle u^2 \rangle$. The volume dependence of F_{vib} is directly related to the vibrational thermal pressure, which we combine with previously reported theoretical values for the electronic and anharmonic thermal pressures to find the total thermal pressure (P_{th}). In addition, we obtained the shape of ε-Fe's melting curve from the volume dependence of our $\langle u^2 \rangle$, and anchored it with an experimentally determined melting point to obtain the high-pressure melting behavior of ε-Fe. Considering thermal pressure and anharmonic effects, we found ε-Fe's melting temperature at the pressure of Earth's core–mantle boundary ($P = 135$ GPa) to be 3500 ± 100 K. Extrapolating our melting curve to the pressure of the inner-core boundary (ICB, $P = 330$ GPa), where Earth's solid inner-core and liquid outer-core are in contact, we determined a melting temperature for ε-Fe of 5600 ± 200 K. Finally, combining this temperature constraint with our P_{th}, we determined the density of ε-Fe under ICB conditions to be 13.50 ± 0.03 g/cm^3, which is 5.5 ± 0.2% higher than the seismically inferred density at the ICB.

© 2011 Elsevier B.V. All rights reserved.

1. Introduction

The Earth's core is thought to be composed mainly of iron with some light elements (McDonough, 2003). Therefore, an accurate determination of the high-pressure phase diagram of iron is of fundamental importance for studies of the deep Earth. Of particular interest is iron's high-pressure melting behavior (e.g., Williams et al., 1987; Boehler, 1993; Shen et al., 1998; Ahrens et al., 2002; Ma et al., 2004; Nguyen and Holmes, 2004), because Earth's solid inner-core and liquid outer-core are in contact at the inner-core boundary. This phase boundary serves as an important constraint on the temperature profile of the core and offers insight into the temperature at the core–mantle boundary, which is a key parameter for geodynamic modeling and for determining what phases are stable in the lowermost mantle.

Existing data suggest that hexagonal close-packed iron (ε-Fe) is the stable phase at core pressures and room temperature (Alfè et al., 2001; Ma et al., 2004; Dewaele et al., 2006; Tateno et al., 2010). However, the high-pressure melting behavior of ε-Fe is not well established due to experimental challenges at simultaneous high-pressure and temperature (*PT*) (e.g., see Fig. 1 in (Nguyen and Holmes, 2004)), which also make it difficult to confirm or reproduce past experimental results.

An alternative to investigating the melting curve of ε-Fe with high-*PT* experiments is to measure its ambient temperature phonon density of states (DOS), which contains vibrational information that is coupled with its melting behavior. In particular, the phonon DOS of ε-Fe is directly related to its mean-square displacement of atoms, which can be used to determine the shape of ε-Fe's high-pressure melting curve. By anchoring this shape with an experimentally determined melting point, one obtains ε-Fe's high-pressure melting behavior from room temperature phonon DOS experiments. This approach minimizes the potential for chemical reactions in high-*PT* experiments and the need to rely on accurate temperature readings at extreme conditions. We present the shape of ε-Fe's high-pressure melting curve, which we benchmark through existing experimental data on ε-Fe.

An additional geophysical application of ε-Fe's room temperature phonon DOS is the direct determination of the volume- and temperature-dependent vibrational free energy, which is related to the vibrational component of the thermal pressure. Together with the electronic and anharmonic components, this gives the total thermal pressure (P_{th}), which is an important parameter for

* Corresponding author. Tel.: +1 626 395 6974; fax: +1 626 564 0715.
E-mail address: caitlinm@caltech.edu (C.A. Murphy).
[1] Present address: Jet Propulsion Laboratory, 4800 Oak Grove Drive, Pasadena, CA 91109, USA.

0031-9201/$ - see front matter © 2011 Elsevier B.V. All rights reserved.
doi:10.1016/j.pepi.2011.07.001

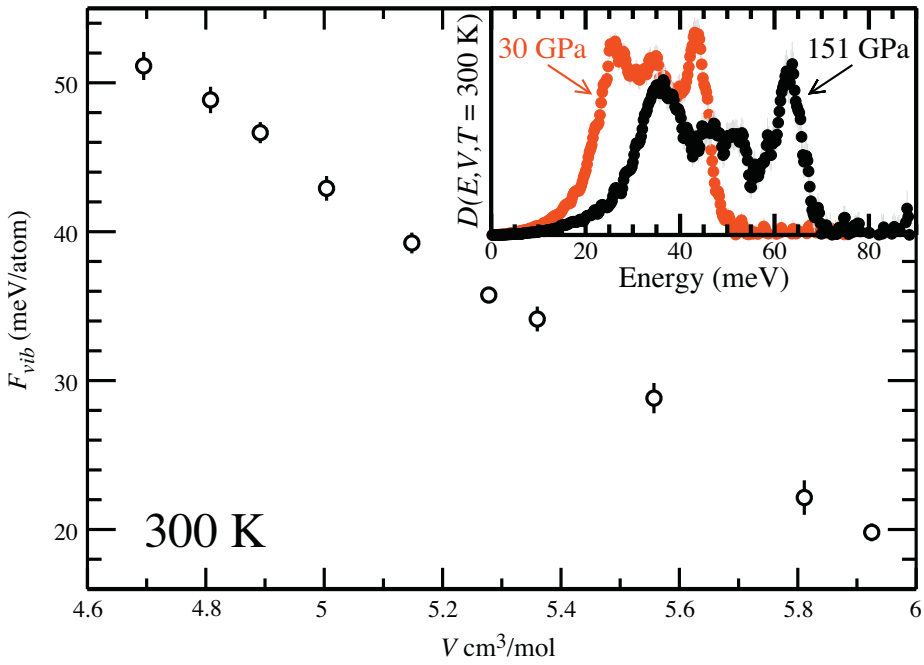

Fig. 1. The volume-dependent vibrational free energy per ^{57}Fe atom (F_{vib}) at 300 K. Inset shows the measured total phonon DOS of ε-Fe at 30 GPa (red) and 151 GPa (black) at 300 K. (For interpretation of the references to color in this figure legend, the reader is referred to the web version of this article.)

determining the density of iron under core conditions. Shock-compression experiments have accessed P_{th} via the thermodynamic Grüneisen parameter and Mie–Grüneisen theory (Jeanloz, 1979; Brown and McQueen, 1986; Asimow and Ahrens, 2010), and many past theoretical calculations have dealt with P_{th} (Wasserman et al., 1996; Stixrude et al., 1997; Vočadlo et al., 2000; Alfè et al., 2001; Sha and Cohen, 2010). Here we present a direct determination of the vibrational component of the thermal pressure from measurements of ε-Fe's phonon DOS.

We performed nuclear resonant inelastic X-ray scattering (NRIXS) and *in situ* synchrotron X-ray diffraction (XRD) experiments in order to directly probe the volume dependence of ε-Fe's total phonon DOS between pressures of 30 GPa and 151 GPa. Similar NRIXS experiments have previously been performed on ε-Fe up to 153 GPa (Lübbers et al., 2000; Mao et al., 2001; Giefers et al., 2002; Shen et al., 2004; Lin et al., 2005). However, these reports did not attempt analysis of the melting curve shape or the determination of the volume-dependent thermal pressure of ε-Fe. In addition, our long data collection times at pressures over 100 GPa resulted in the highest statistical quality phonon DOS to outer-core pressures measured to date, and our *in situ* determination of sample volume with XRD distinguishes this study from previous similar works.

2. Experimental methods

We prepared three modified panoramic diamond anvil cells (DACs) with 90° openings on the downstream side and beveled anvils with flat culet diameters of 250 μm or 150 μm. For each DAC, a piece of 10 μm thick 95% enriched ^{57}Fe foil was loaded into a beryllium gasket with a boron epoxy insert that stabilized the gasket hole during compression. For measurements made at atomic volumes of ε-Fe greater than 5.27 cm^3/mol (P_V < 77 GPa), Ne was loaded as the pressure transmitting medium at the GeoSoilEnviroCARS sector of the Advanced Photon Source (APS) at Argonne National Laboratory, using our gear box for gas-loading panoramic DACs. For measurements made at atomic volumes of 5.27 cm^3/mol and smaller, the ^{57}Fe foil was fully embedded in the boron epoxy which served as the pressure transmitting medium.

NRIXS experiments were performed at beamline 3-ID-B of the APS, and the storage ring was operated in top-up mode with 24 bunches that were separated by 153 ns. Three avalanche photodiode detectors (APDs) were positioned radially around and close to the sample in order to collect the incoherent inelastic scattered photons. A fourth APD was positioned downstream in the forward scattering direction and independently measured an average energy resolution (ΔE) of 1.2 meV at FWHM. The high-resolution monochromator was tuned from −65 meV to +85 meV around the nuclear resonance energy of ^{57}Fe (14.4125 keV), with a step size of 0.25 meV and a collection time of 5 s per energy step. Between 8 and 21 NRIXS scans were collected for each compression point, with the exception of our measurement at 5.81 cm^3/mol (P_V = 36 GPa), for which only four scans were collected.

XRD data collected *in situ* before and after each NRIXS dataset at the same sample position were averaged in order to determine the atomic volume (λ = 0.086 nm, E = 14.4125 keV). XRD image plate data was analyzed with the Fit2D software (Hammersley et al., 1996), and the Fityk software (Wojdyr, 2010) was used to determine the a and c lattice parameters at each compression point by fitting Gaussians to the observed (100), (002), and (101) diffraction peaks. For our determination of the phonon DOS and data analysis, we relied on our *in situ* measured volumes. To present our results on a common pressure scale and for discussion, we converted our measured volumes to pressures (P_V) using the Vinet equation of state (EOS) for ε-Fe (Dewaele et al., 2006) (Table 1). Most compression points had volume errors of 0.1% and corresponding pressure uncertainties of 1 GPa. However, our measurement at 4.89 cm^3/mol (P_V = 121 GPa) had a volume error of 0.5% and a corresponding pressure uncertainty of 2 GPa.

For our four largest compression points, we observed some texturing in the form of a loss of intensity in the (002) diffraction peak (Table 1), likely due to non-hydrostatic conditions at extreme pressures. To evaluate the sensitivity of our results to

Table 1
NRIXS and *in situ* XRD experimental results, with melting temperatures and thermal pressures determined from the phonon DOS.

V (cm^3/mol)[a]	ρ (g/cm^3)[a]	P_V (GPa)[a]	F_{vib} (meV/atom)[b]	T_{LM} (K)[b]	T_M^h (K)[c]	P_{th} (GPa)[d]	T_M (K)[c]
5.92(2)	9.61(3)	30(2)	19.8(6)	2140(20)	2470(70)	17(1)	2190
5.81(1)	9.80(1)	36(2)	22(1)	2210(40)	2520(80)	18(1)	2250
5.56(1)	10.25(1)	53(3)	29(1)	2520(40)	2790(90)	22(1)	2600
5.36(1)	10.63(1)	69(4)	34.1(8)	2810(30)	3040(90)	25(1)	2940
5.27(2)	10.80(2)	77(5)	35.7(5)	2920(20)	3130(90)	27(1)	3110
5.15(2)	11.06(2)	90(5)	39.2(7)	3180(30)	3300(100)	30(1)	3400
5.00(2)*	11.38(2)	106(6)	42.9(8)	3370(30)	3500(100)	31(1)	3520
4.89(2)*	11.64(5)	121(8)	46.7(7)	3660(40)	3700(100)	35(2)	3880
4.81(2)*	11.84(2)	133(8)	48.8(9)	3830(50)	3900(100)	36(2)	3930
4.70(2)*	12.13(3)	151(9)	51.1(9)	4130(60)	4100(100)	39(2)	4160

Note: Values in parentheses denote errors for the last significant digit(s) reported.
* Texturing was observed at these compressions in the form of a loss of intensity in the (002) diffraction peak. See Section 2 for more discussion.
[a] Volume (V) and density (ρ) were measured with XRD and converted to pressure (P_V) using the Vinet EOS. Errors in P_V account for uncertainties in EOS parameters (Dewaele et al., 2006).
[b] The vibrational free energy (F_{vib}) and Lamb–Mössbauer temperature (T_{LM}) at 300 K were calculated from the measured total phonon DOS (Sturhahn, 2000, 2004).
[c] The harmonic melting temperatures (T_M^h) were determined using Eq. (9) and the Ma et al. (2004) anchor melting point; anharmonic melting temperatures (T_M) account for anharmonic effects (see Appendix A).
[d] The total thermal pressure (P_{th}) was taken at T_M and used in Eq. (10) before extrapolating and plotting T_M (P) in Fig. 3.

possible effects from texturing, we re-evaluated the volumes of our four largest compression points with an assigned c/a ratio from Dewaele et al.'s (2006) static-compression XRD study to over 200 GPa, in which He and Ne were used as pressure transmitting media. With the exception of our measurement at 5.00 cm^3/mol (P_V = 106 GPa), all resulting volumes and corresponding pressures were within the errors of our original analysis, indicating only a weak effect from texturing.

NRIXS data was analyzed with the PHOENIX software, which was used to remove the elastic contribution and apply the quasi-harmonic lattice model (Sturhahn, 2000; Sturhahn and Jackson, 2007). From the resulting volume-dependent total phonon DOS, $\mathscr{D}(E,V)$, we obtained two parameters that are directly related to ε-Fe's thermal pressure and melting curve shape. The vibrational free energy per ^{57}Fe atom (F_{vib}) is given by

$$F_{vib}(V,T) = \frac{1}{\beta}\int \ln\left(2\sinh\frac{\beta E}{2}\right)\mathscr{D}(E,V)\mathrm{d}E \quad (1)$$

(Table 1, Fig. 1), where β is the inverse temperature, and the mean-square displacement of ^{57}Fe atoms, $\langle u^2\rangle$, is given by

$$\langle u^2\rangle = \frac{E_R}{3k_0^2}\int \frac{1}{E}\coth\frac{\beta E}{2}\mathscr{D}(E,V)dE, \quad (2)$$

where E_R is the recoil energy and k_0 is the wavenumber of the resonant photon. For the 14.4125 keV transition of ^{57}Fe, E_R = 1.956 meV and k_0 = 7.306 Å^{-1} (Sturhahn, 2004).

To demonstrate the high statistical quality of our phonon DOS, we compare our measured uncertainties with those from a previous NRIXS study on ε-Fe over a similar compression range (Mao et al., 2001). Performing the same PHOENIX analysis on both datasets, we find that our data produce errors for parameters determined from the phonon DOS that are ~70% smaller on average (e.g., for F_{vib}), largely due to our long data collection times at large compressions and the higher-resolution monochromator (ΔE = 2 meV in Mao et al. (2001)).

3. Thermal pressure

The total thermal pressure is additive in its vibrational and electronic components:

$$P_{th} = P_{vib} + P_{el} = -\left(\frac{\partial F_{vib}}{\partial V}\right)_T - \left(\frac{\partial F_{el}}{\partial V}\right)_T. \quad (3)$$

Taking the derivative of the best-fit polynomial of our $F_{vib}(V, 300\ \mathrm{K})$ data (Table 1), we directly obtain P_{vib}(300 K) = 2.31 ± 0.06 GPa and 2.70 ± 0.06 GPa at our smallest (30 GPa) and largest (151 GPa) compression points, respectively. We can also investigate the temperature-dependence of P_{vib} using our ambient-temperature data, because F_{vib} is directly proportional to T (see Eq. (1)). However, temperature effects on the phonon DOS have not been accounted for, e.g., softening of phonon energies with increasing temperature, so derivatives of the best-fit polynomials of our $F_{vib}(V,T > 300\ \mathrm{K})$ give only the harmonic component of the vibrational thermal pressure (P_{vib}^h). Therefore, taking T = 5600 K, we find P_{vib}^h (5600 K) = 37 ± 3 GPa and 40 ± 3 GPa at our smallest and largest compression points, respectively, which corresponds to an 8% increase over the volume range of this study.

In order to obtain the total $P_{vib}(V,T)$ for T > 300 K, we must account for the anharmonic component of the vibrational thermal pressure (P_{vib}^{anh}) using

$$P_{vib}(V,T) = P_{vib}^h(V,T) + \left[P_{vib}^{anh}(V,T) - P_{vib}^{anh}(V,300\ \mathrm{K})\right]. \quad (4)$$

Experimental data for temperature effects on ε-Fe's phonon DOS are not available for the PT conditions of interest here, so we rely on theoretical values for P_{vib}^{anh} (V,T). Dewaele et al. (2006) fit *ab initio* anharmonic thermal pressures (Alfè et al., 2001) with the formulation (Dorogokupets and Oganov, 2006)

$$P_{vib}^{anh}(V,T) = A_{vib}^{anh}\left(\frac{V}{V_0}\right)^{B_{vib}^{anh}}T^2, \quad (5)$$

and found $A_{vib}^{anh} = 1.28\times10^{-7}$ GPa K^{-2} and B_{vib}^{anh} = 0.87. Applying Eq. (5) and our P_{vib}^h (V,T) to Eq. (4), we obtain the total $P_{vib}(V,T)$. For T = 5600 K, we find P_{vib}(5600 K) = 41 GPa and 43 GPa at our smallest and largest compression points, respectively (Fig. 2).

Finally, for the volume- and temperature-dependent electronic thermal pressure, we use Dewaele et al.'s (2006) fit of *ab initio* values for $P_{el}(V,T)$ (Alfè et al., 2001) with the formulation given in Eq. (5), where they found $A_{el} = 4.82\times10^{-7}$ GPa K^{-2} and B_{el} = 0.339. Applying our $P_{vib}(V,T)$ and this semi-empirical relationship for $P_{el}(V,T)$ to Eq. (3), we find P_{th}(300 K) = 2.35 GPa and 2.74 GPa, and P_{th}(5600 K) = 55 GPa and 56 GPa at our smallest and largest compression points, respectively (Table 1).

Our $P_{vib}(V,\ 300\ \mathrm{K})$ agree well with Dewaele et al.'s (2006) reported values for the quasi-harmonic Debye thermal pressure. In addition, our P_{vib}^h (V,T) agree fairly well with Alfè et al.'s (2001) *ab initio* density-functional theory (DFT) calculations of the high-temperature harmonic thermal pressure, although they reported a faster increase in P_{vib}^h with decreasing volume (~20% over the volume range of this study). Therefore, an experimental determina-

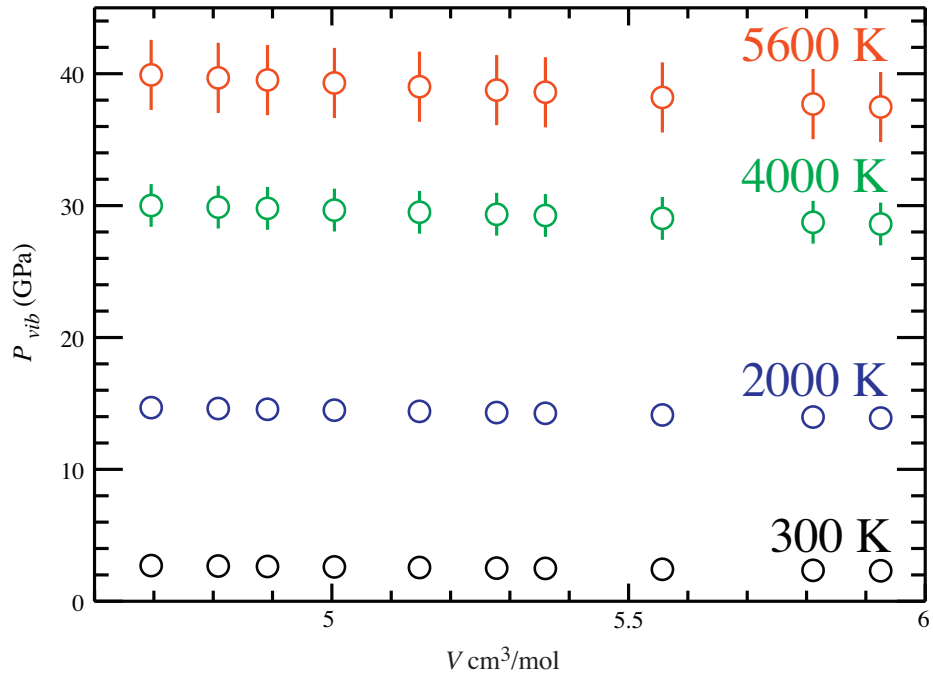

Fig. 2. The volume- and temperature-dependent vibrational thermal pressure (P_{vib}) of ε-Fe. $P_{vib}(T > 300\ \mathrm{K})$ account for anharmonic effects, and errors calculated from best-fit parameters are smaller than the symbol if not visible.

tion of $P^h_{vib}(V,T)$ agrees qualitatively with select first principles calculations. Finally, our $P_{th}(V,T)$ are in excellent agreement with a DFT calculation by Vočadlo et al. (2000), but our observed trend is opposite to that predicted by Sha and Cohen (2010) in their DFT calculation of P_{th} for ε-Fe.

4. High-pressure melting behavior

To constrain the high-pressure melting curve of ε-Fe, we start with Gilvarry's reformulation of Lindemann's original melting relation (Gilvarry, 1956a), which is thought to be a good approximation for the shape of the melting curves of close-packed, monatomic materials, such as ε-Fe (Mulargia and Quareni, 1988; Poirier, 2000). This formulation states that melting occurs when the mean-square displacement of atoms, $\langle u^2\rangle$, reaches a critical fraction (C) of the mean-square separation of nearest neighbor atoms, $\langle r^2\rangle$ (Gilvarry, 1956a), or

$$\langle u^2\rangle = C\langle r^2\rangle. \tag{6}$$

We have defined $\langle u^2\rangle$ above (Eq. (2)), and now present its high-temperature formulation

$$\langle u^2\rangle \approx k_B T \frac{2E_R}{3k_0^2}\int \frac{1}{E^2}\mathscr{D}(E,V)dE \equiv \frac{T}{k_0^2}\frac{1}{T_{LM}}, \tag{7}$$

where k_B is Boltzmann's constant, and the Lamb–Mössbauer temperature (T_{LM}) is introduced for discussion and to simplify the expression (Table 1). Eq. (7) is valid for $k_BT \gg E_{max}$, where E_{max} is the maximum (cutoff) energy of the phonon DOS. For our smallest and largest compression points, E_{max} is ~50 meV and ~70 meV, respectively (see inset in Fig. 1). If we predict an E_{max} at 330 GPa and 300 K of ~100 meV, then this high-temperature approximation for $\langle u^2\rangle$ is valid for $T \gg 1200$ K, which is well below the melting temperatures discussed here.

Substituting Eq. (7) into Eq. (6) and rearranging, we obtain an expression for the harmonic melting temperature (T^h_M) that is based on our measured phonon DOS via $T_{LM}(V)$:

$$T^h_M(V) \approx k_0^2 C\langle r^2\rangle \cdot T_{LM}(V). \tag{8}$$

The value of k_0 does not depend on volume, C is thought to be approximately constant with volume (Gilvarry, 1956b), and $\langle r^2\rangle \propto V^{2/3}$ for an hcp unit cell, so we rewrite Eq. (8) in a reduced states form as

$$T^h_M(V) = T_{M0}\cdot\left(\frac{V}{V_{M0}}\right)^{2/3}\frac{T_{LM}(V)}{T_{LM}(V_{M0})}. \tag{9}$$

From Eq. (9), our $T_{LM}(V)$ determines the shape of ε-Fe's melting curve, but an anchor melting point (represented by T_{M0} and V_{M0}) is necessary to calibrate the melting temperatures. For the anchor melting point, we use $T_M(P = 105\ \mathrm{GPa}) = 3510 \pm 100$ K for ε-Fe, which was measured by Ma et al. (2004) using laser-heated static compression *in situ* synchrotron XRD. We convert their reported pressure to volume using the Vinet EOS (Dewaele et al., 2006), and determine $T_{LM}(V_{M0})$ by quadratic interpolation of our measured $T_{LM}(V)$. Applying these anchor point values and our measured $T_{LM}(V)$ to Eq. (9), we find $T^h_M = 2470 \pm 70$ K and 4100 ± 100 K at our smallest and largest compression points, respectively (Table 1). Reported errors account for measured uncertainties in V and T_{LM}, and an uncertainty in T_{M0} of 100 K (Ma et al., 2004).

5. Discussion

Our harmonic melting points are based on room temperature measurements of the phonon DOS, and therefore do not account for thermal pressure or non-harmonic effects. To find the total pressure at each melting point, we apply our $P_{th}(V,T)$ to the high-*PT* EOS:

$$P(V,T_M) = P_V(V,300K) + [P_{th}(V,T_M) - P_{th}(V,300\ \mathrm{K})]. \tag{10}$$

P_V is the pressure determined by applying the Vinet EOS (Dewaele et al., 2006) to our measured volumes, and the square brackets contain our thermal pressure correction, which already accounts for anharmonic effects (see Section 4).

We now approximate an anharmonic correction term for our melting temperatures by investigating the temperature dependence of T_{LM}. We assume that the phonon DOS scales regularly with temperature, and that the temperature derivatives of the seismic velocity and the Debye sound velocity at constant volume are directly related (Appendix A). Combined with thermodynamic definitions, these assumptions give rise to an anharmonic correction term of –11% at our smallest compression point, or an anharmonic melting temperature (T_M) of ~2190 K (Appendix A). This anharmonic correction decreases at larger compressions, and for $P \geqslant 100$ GPa after accounting for P_{th}, our anharmonic melting temperatures are within the errors of our $T_M^h(V)$ (Table 1). The one exception, where T_M(4.89 cm^3/mol) exceeds T_M^h (4.89 cm^3/mol) by more than its error, may be related to the volume uncertainty of that compression point.

At the pressure of the core-mantle boundary, we find T_M(135 GPa) = 3500 ± 100 K. To benchmark this result, we find that it agrees well with Ahrens et al.'s (2002) shock-compression study, in which they found T_M(135 GPa) = 3400 ± 200 K. In addition, it agrees fairly well with Boehler's (1993) T_M(135 GPa) = 3200 ± 100 K (see Fig. 2a in reference), which was determined by the onset of convective motion in laser-heated static-compression experiments. However, our melting temperature lies well below that reported by Williams et al. (1987), who found T_M(135 GPa) = 4800 ± 200 K using a combination of static- and shock-compression experiments.

To extrapolate our melting results beyond the compression range of this study, we apply two independent extrapolation equations. First, we use the Simon–Glatzel equation (Simon and Glatzel, 1929), which is an empirical relation for the pressure dependence of T_M given by

$$T_M = T_{M0}\left(\frac{P_M - P_{M0}}{x} + 1\right)^y, \tag{11}$$

where x and y are fitting parameters. For the anchor melting point (T_{M0} and P_{M0}), we again use the result from Ma et al. (2004), but we first apply our thermal pressure correction since thermal pressure was not accounted for in their study. Using Eq. (11) to fit and extrapolate our melting points, which account for thermal pressure and anharmonic effects, we find a melting temperature at the inner-core boundary (ICB, P = 330 GPa) of 5700 ± 100 K (Fig. 3). Here we have assigned the error to be that of our largest compression point's harmonic melting temperature, which is slightly larger than the error derived from fitting parameter uncertainties.

The second extrapolation equation is a commonly used approximate form of Lindemann's melting relation:

$$T_M(V) = T_{M0}\exp\left[2\gamma_{M0}\left(1 - \frac{V}{V_{M0}}\right) + \frac{2}{3}\ln\left(\frac{V}{V_{M0}}\right)\right] \tag{12}$$

(Poirier, 2000), where the vibrational Grüneisen parameter at the volume of the anchor melting point (γ_{M0}) serves as the fitting parameter. Taking T_{M0} and V_{M0} from Ma et al. (2004), we fit our ten melting points with Eq. (12) and find γ_{M0} = 1.65 ± 0.06. We then simultaneously solve for $P(V,T_M)$ and $T_M(V)$ (Eqs. (10) and (12)) in order to determine the volume of ε-Fe at the pressure of the ICB that accounts for the melting temperature-dependent thermal pressure. The result is a self-consistent melting temperature for ε-Fe at 330 GPa of 5500 ± 100 K, where the error is assigned as before.

Combining the results of our two independent extrapolations, we find the melting temperature of ε-Fe at the ICB to be T_M(330 GPa) = 5600 ± 200 K. To further benchmark this result and investigate its sensitivity to the anchor melting point, we perform the same thermal pressure correction, anharmonic correction, and extrapolation procedures with alternate anchor melting points. Anchoring our melting curve shape with the triple

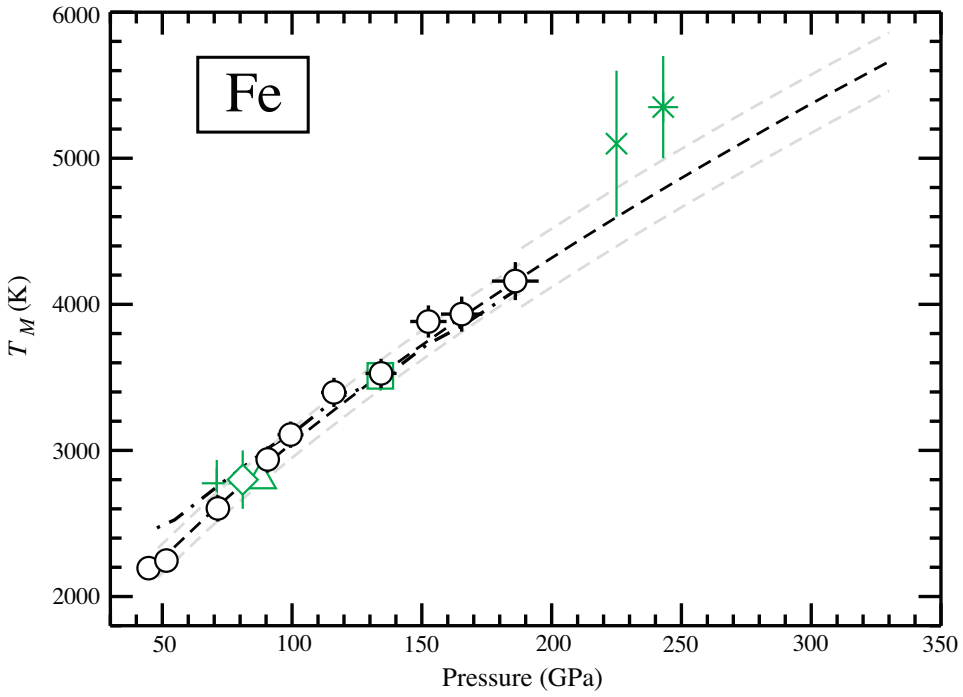

Fig. 3. The high-pressure melting behavior of ε-Fe. Black circles show melting points that account for thermal pressure and anharmonic effects. The black dashed line gives the fit and extrapolation of our melting points with Eq. (11), and the gray dashed lines show uncertainties of ±100 K over our experimental compression range, and ±200 K beyond our compression range. The black dash-dotted line shows our harmonic melting temperatures, which account for thermal pressure. The green x, +, and ∗ show results from shock-compression melting experiments by Nguyen and Holmes (2004), Ahrens et al. (2002), and Brown and McQueen (1986), respectively; the green triangle, square, and diamond show results from static-compression XRD experiments by Komabayashi and Fei (2010), Ma et al. (2004), and Shen et al. (1998), respectively, where the final two have been corrected to account for thermal pressure following Eq. (10). (For interpretation of the references to color in this figure legend, the reader is referred to the web version of this article.)

point measured by Shen et al. (1998) at 81 GPa (after accounting for P_{th}) and 2800 K, we find T_M(330 GPa) ~5500 K to 5800 K. In addition, anchoring our melting curve shape with Komabayashi and Fei's (2010) determined triple point at 88 GPa and 2800 K, we find T_M(330 GPa) ~5300 K from Eq. (11), and ~5300 K from Eq. (12). Therefore, using the shape we determine from the phonon DOS, the melting temperature of ε-Fe at the ICB predicted from Ma et al.'s (2004) melting point, Shen et al.'s (1998) triple point, and Komabayashi and Fei's (2010) triple point all agree within their uncertainties, thus serving as benchmarks for our approach.

Finally, we note that considering the uncertainties of our melting curve shape and our two independent extrapolations, our results intersect the range of values reported in the shock-compression studies of Nguyen and Holmes (2004) and Brown and McQueen (1986) (Fig. 3).

From Eq. (10), our $P_{th}(V,T)$, and our T_M(330 GPa) = 5600 ± 200 K, we find the density of pure ε-Fe to be ρ_{Fe}(330 GPa) = 13.50 ± 0.03 g/cm^3. This ρ_{Fe} can also be reported as a core density deficit (CDD), or the percent difference between the density of ε-Fe under core conditions and the seismically inferred density of the core. The preliminary reference Earth model (PREM) predicts a density at the ICB of 12.76 g/cm^3, based on observations of Earth's normal modes and seismic wave travel times (Dziewonski and Anderson, 1981). Together with our ρ_{Fe}(330 GPa, 5600 ± 200 K), this gives a CDD of 5.5 ± 0.2%, where the uncertainty reflects the errors we assigned to our extrapolated melting temperatures. Our CDD value agrees well with Komabayashi and Fei's (2010) recently calculated CDD of 5.3 wt.%, which is based on static-compression experiments and a lower melting temperature for ε-Fe at the ICB.

The CDD offers insight into the amount of light elements present in the core (Poirier, 2000; Hemley and Mao, 2001). However, the alloying of Ni and light elements (e.g., S, Si, O, C, H) may affect the melting temperature and other thermoelastic parameters of ε-Fe (e.g., Boehler, 1992; Poirier, 2000; Seagle et al., 2008) and in turn, complicate the determination of the true composition of the core by, for example, altering the P_{th} correction. In order to better constrain the CDD, it would be ideal to use the density of an Fe–Ni alloy at ICB conditions as a reference, rather than pure Fe. While the EOS of Fe–Ni is thought to be similar to that of pure Fe (Mao et al., 1990), the effect of alloying on P_{th} is not well known.

To summarize, we determined ε-Fe's high-pressure melting behavior and thermal pressure from room temperature measurements of its total phonon DOS. Accounting for thermal pressure and anharmonic effects, we found ε-Fe's melting temperature at the pressure of the CMB to be 3500 ± 100 K. In addition, by combining the results of two independent extrapolations of our melting curve, we found ε-Fe's melting temperature at the ICB to be 5600 ± 200 K. We have presented benchmarking cases and show that the melting temperatures of ε-Fe predicted from our approach are in agreement with shock-compression studies. Finally, our predicted melting temperature for ε-Fe at the ICB corresponds to a CDD of 5.5 ± 0.2%.

Acknowledgements

We would like to thank D. Zhang, H. Yavas, and J.K. Wicks for assistance during the experiments, and NSF-EAR-0711542, NSF-CAREER-0956166, and Caltech for support of this research. We thank two anonymous reviewers for their comments that helped to improve our manuscript. Use of the Advanced Photon Source was supported by the U.S. D.O.E., O.S., O.B.E.S. (DE-AC02-06CH11357). Sector 3 operations are supported in part by COMPRES (NSF EAR 06-49658).

Appendix A. Details of melting temperature calculation

Relevant parameters for determining the high-pressure melting behavior of ε-Fe with Eqs. (9)–(12) and the Ma et al. (2004) anchor melting point are given in Table A.1. To approximate an anharmonic correction term for our harmonic melting temperatures, we begin with the hypothesis that ε-Fe's phonon DOS scales regularly with temperature:

$$\mathscr{D}(E,V,T) = \xi(V,T)\mathscr{D}(\xi(V,T)E, V_0, T_0), \tag{A.1}$$

where the scaling parameter (ξ) is independent of energy and $\xi(V_0,T_0) = 1$. Together with the low-energy Debye-like description of the phonon DOS (Hu et al., 2003), Eq. (A.1) gives

$$\frac{\xi^3(V,T)\,v_D^3(V,T)}{V} = \frac{v_D^3(V_0,T_0)}{V_0}, \tag{A.2}$$

where v_D is the Debye sound velocity, and the subscript 0 refers to some reference conditions.

Next, we write the temperature derivatives of v_D and the seismic velocity (v_ϕ) at constant volume, which are given by

$$\begin{aligned} 3v_D^{-3}\left(\frac{\partial \ln v_D}{\partial \ln T}\right)_V &= v_P^{-3}\left(\frac{\partial \ln v_P}{\partial \ln T}\right)_V + 2v_S^{-3}\left(\frac{\partial \ln v_S}{\partial \ln T}\right)_V \\ v_\phi^2\left(\frac{\partial \ln v_\phi}{\partial \ln T}\right)_V &= v_p^2\left(\frac{\partial \ln v_p}{\partial \ln T}\right)_V - \frac{4}{3}v_s^2\left(\frac{\partial \ln v_s}{\partial \ln T}\right)_V, \end{aligned} \tag{A.3}$$

where v_P and v_S are the compressional and shear sound velocities, respectively. The derivatives in Eq. (A.3) are related by

$$\left(\frac{\partial \ln v_D}{\partial \ln T}\right)_V = \left(\frac{\partial \ln v_\phi}{\partial \ln T}\right)_V \frac{3-4\eta^2}{2+\eta^3}\frac{2\Psi+\eta^3}{3-4\Psi\eta^2}, \tag{A.4}$$

where $\eta = v_S/v_P$, and $\psi = (\partial \ln v_S/\partial \ln T)_V/(\partial \ln v_P/\partial \ln T)_V$. There is also a direct relationship between v_ϕ and the isothermal bulk modulus (K_T), so we find

$$\begin{aligned} \left(\frac{\partial \ln v_\phi}{\partial \ln T}\right)_V &= \frac{1}{2}\alpha T\left(K_T' + \frac{\gamma}{(1+\alpha\gamma T)} - \delta_T\right) \\ &\approx \frac{1}{2}\alpha T(K_T' + \gamma - \delta_T), \end{aligned} \tag{A.5}$$

where α is the thermal expansion coefficient, K_T' is the pressure derivative of K_T, δ_T is the Anderson–Grüneisen parameter, and γ is the thermodynamic Grüneisen parameter.

Combining Eq. (A.2), (A.4), and (A.5), we obtain an expression for the temperature derivative of the scaling parameter at constant volume:

Table A.1
Anchor melting point parameters for determining the high-pressure melting behavior of ε-Fe with Eqs. (9)–(12).[a]

	Ma et al. (2004)
T_{M0} (K)	3510(100)
V_{M0} (cm^3/mol)	5.01
P_{M0} (GPa)	134
$T_{LM}(V_{M0})$ (K)	3390
x	160(40)
y	0.6(1)
γ_{M0}	1.65(6)

[a] Parameters are calculated for the melting point measured by Ma et al. (2004), as described in the text. P_{M0} accounts for thermal pressure, parameters x and y are from Eq. (11), and γ_{M0} is from Eq. (12).

Table A.2
Anharmonic correction term parameters (see Eq. (A.8)).[a]

V (cm^3/mol)	α (10^{-5} K^{-1})	K'_T	δ_T	γ	Ψ
5.92(2)	3.88	4.47	4.91	1.68	1.97
5.81(1)	3.65	4.37	4.86	1.65	2.02
5.56(1)	3.06	4.17	4.73	1.61	2.15
5.36(1)	2.59	4.03	4.64	1.57	2.26
5.27(2)	2.45	3.97	4.59	1.56	2.31
5.15(2)	2.11	3.89	4.53	1.54	2.38
5.00(2)	1.81	3.80	4.46	1.52	2.45
4.89(2)	1.60	3.73	4.40	1.50	2.51
4.81(2)	1.43	3.68	4.36	1.49	2.54
4.70(2)	1.27	3.62	4.31	1.48	2.57

[a] α is the thermal expansion coefficient (Anderson et al., 2001); K'_T is the pressure derivative of K_T (Dewaele et al., 2006); δ_T is the Anderson–Grüneisen parameter (Sharma and Sharma, 2010); γ is the Grüneisen parameter (Dewaele et al., 2006); and ψ is the ratio of the logarithmic temperature derivatives of v_S and v_P at constant volume (Stacey and Davis, 2004).

$$\left(\frac{\partial \ln \xi}{\partial \ln T}\right)_V = -\frac{1}{2}\alpha T(K'_T + \gamma - \delta_T)\frac{3-4\eta^2}{2+\eta^3}\frac{2\Psi+\eta^3}{3-4\Psi\eta^2} \equiv -\frac{1}{2}\alpha T\epsilon, \tag{A.6}$$

where ϵ is introduced for abbreviation. Reasonable values of ψ over the compression range of this study are between 2 and 2.6 (Stacey and Davis, 2004), and previously reported values for v_P and v_S indicate $\eta \sim 0.5$ for ε-Fe (Mao et al., 2001; Lin et al., 2005).

Assuming $\alpha\epsilon$ varies with volume but not temperature, we are then able to integrate Eq. (A.6) and obtain the following expression for the anharmonic melting temperature (T_M):

$$T_M = T_M^h \exp\left[\alpha\epsilon(T_M - T_0) - \alpha_{M0}\epsilon_{M0}(T_{M0} - T_0)\right]. \tag{A.7}$$

T_M^h is the uncorrected harmonic melting temperature (Eq. (9)); $\alpha_{M0} = \alpha(V_{M0})$ and $\epsilon_{M0} = \epsilon(V_{M0})$, where V_{M0} is the volume of the anchor melting point; T_{M0} is the melting temperature of the anchor melting point; and $T_0 = 300$ K, the temperature at which our experiments were performed. Finally, since we find $|\alpha\epsilon(T_M - T_{M0})| \ll 1$, we can approximate the exponential linearly and solve for T_M:

$$T_M \approx T_M^h \frac{(1-\alpha\epsilon T_{M0})\exp[(\alpha\epsilon - \alpha_{M0}\epsilon_{M0})(T_{M0} - T_0)]}{1 - \alpha\epsilon T_M^h \exp[(\alpha\epsilon - \alpha_{M0}\epsilon_{M0})(T_{M0} - T_0)]}. \tag{A.8}$$

We use Eq. (A.8) to determine our anharmonic melting temperatures, and the collection of terms to the right of T_M^h in Eq. (A.8) are what we call the "anharmonic correction term." Taking $\eta = 0.5$, $\psi(V)$ from Stacey and Davis (2004), δ_T from Sharma and Sharma (2010), and K'_T and γ from Dewaele et al. (2006) (Table A.2), we find that $\epsilon(V)$ varies between 4.6 and 9.0 over the compression range of this study. Finally, applying these $\epsilon(V)$ values and $\alpha(V)$ from Anderson et al. (2001), we find an anharmonic correction term of 0.89 at our smallest compression point. For $P \geqslant 100$ GPa (after accounting for thermal pressure), this correction term is ~1.

References

Ahrens, T.J., Holland, K.G., Chen, G.Q., 2002. Phase diagram of iron, revised-core temperatures. Geophys. Res. Lett. 29, 4.

Alfè, D., Price, G.D., Gillan, M.J., 2001. Thermodynamics of hexagonal-close-packed iron under Earth's core conditions. Phys. Rev. B 64, 16.

Anderson, O.L., Dubrovinsky, L., Saxena, S.K., LeBihan, T., 2001. Experimental vibrational Gruneisen ratio values for epsilon-iron up to 330 GPa at 300 K. Geophys. Res. Lett. 28, 399–402.

Asimow, P.D., Ahrens, T.J., 2010. Shock compression of liquid silicates to 125 GPa: the anorthite-diopside join. J. Geophys. Res. Solid Earth 115.

Boehler, R., 1992. Melting of the Fe–FeO and the Fe–FeS systems at high pressure: constraints on core temperatures. Earth Planet. Sci. Lett. 111, 217–227.

Boehler, R., 1993. Temperatures in the Earth's core from melting point measurements of iron at high static pressures. Nature 363, 534–536.

Brown, J.M., McQueen, R.G., 1986. Phase transitions, Grüneisen parameter, and elasticity for shocked iron between 77 GPa and 400 GPa. J. Geophys. Res. Solid Earth Planets 91, 7485–7494.

Dewaele, A., Loubeyre, P., Occelli, F., Mezouar, M., Dorogokupets, P.I., Torrent, M., 2006. Quasihydrostatic equation of state of iron above 2 Mbar. Phys. Rev. Lett. 97, 4.

Dorogokupets, P.I., Oganov, A.R., 2006. Equations of state of Al, Au, Cu, Pt, Ta, and W and revised ruby pressure scale. Dokl. Earth Sci. 410, 1091–1095.

Dziewonski, A.M., Anderson, D.L., 1981. Preliminary reference Earth model. Phys. Earth Planet. Inter. 25, 297–356.

Giefers, H., Lübbers, R., Rupprecht, K., Wortmann, G., Alfè, D., Chumakov, A.I., 2002. Phonon spectroscopy of oriented hcp iron. High Pressure Res. 22, 501–506.

Gilvarry, J.J., 1956a. The Lindemann and Grüneisen laws. Phys. Rev. 102, 308–316.

Gilvarry, J.J., 1956b. Variation of the amplitude of thermal vibration on the fusion curve. Phys. Rev. 104, 908–913.

Hammersley, A.P., Svensson, S.O., Hanfland, M., Fitch, A.N., Häusermann, D., 1996. Two-dimensional detector software: from real detector to idealised image or two-theta scan. High Pressure Res. 14, 235–248.

Hemley, R.J., Mao, H.K., 2001. In situ studies of iron under pressure: new windows on the Earth's core. Int. Geol. Rev. 43, 1–30.

Hu, M.Y., Sturhahn, W., Toellner, T.S., Mannheim, P.D., Brown, D.E., Zhao, J.Y., Alp, E.E., 2003. Measuring velocity of sound with nuclear resonant inelastic X-ray scattering. Phys. Rev. B 67, 5.

Jeanloz, R., 1979. Properties of iron at high pressures and the state of the core. J. Geophys. Res. 84, 6059–6069.

Komabayashi, T., Fei, Y.W., 2010. Internally consistent thermodynamic database for iron to the Earth's core conditions. J. Geophys. Res. Solid Earth 115, 12.

Lin, J.F., Sturhahn, W., Zhao, J.Y., Shen, G., Mao, H.K., Hemley, R.J., 2005. Sound velocities of hot dense iron: Birch's law revisited. Science 308, 1892–1894.

Lübbers, R., Grünsteudel, H.F., Chumakov, A.I., Wortmann, G., 2000. Density of phonon states in iron at high pressure. Science 287, 1250–1253.

Ma, Y.Z., Somayazulu, M., Shen, G., Mao, H.K., Shu, J.F., Hemley, R.J., 2004. In situ X-ray diffraction studies of iron to Earth-core conditions. Phys. Earth Planet. Inter. 143, 455–467.

Mao, H.K., Wu, Y., Chen, L.C., Shu, J.F., Jephcoat, A.P., 1990. Static Compression of Iron to 300 GPa and $Fe_{0.8}Ni_{0.2}$ alloy to 260 GPa: implications for composition of the core. J. Geophys. Res. Solid Earth Planets 95, 21737–21742.

Mao, H.K., Xu, J., Struzhkin, V.V., Shu, J., Hemley, R.J., Sturhahn, W., Hu, M.Y., Alp, E.E., Vočadlo, L., Alfè, D., Price, G.D., Gillan, M.J., Schwoerer-Böhning, M., Häusermann, D., Eng, P., Shen, G., Giefers, H., Lübbers, R., Wortmann, G., 2001. Phonon density of states of iron up to 153 gigapascals. Science 292, 914–916.

McDonough, W.F. 2003. Compositional model for the Earth's core. In: Carlson, R.W. (Ed.), The Mantle and Core. In: Holland, H.D., Turekian, K.K. (Eds.), Treatise on Geochemistry. Elsevier-Pergamon, Oxford, pp. 547–568.

Mulargia, F., Quareni, F., 1988. Validity of the Sutherland–Lindemann law and melting temperatures in the Earth's interior. Geophys. J. Oxf. 92, 269–282.

Nguyen, J.H., Holmes, N.C., 2004. Melting of iron at the physical conditions of the Earth's core. Nature 427, 339–342.

Poirier, J.-P., 2000. Introduction to the Physics of the Earth's Interior, second ed. Cambridge University Press, Cambridge, UK.

Seagle, C.T., Heinz, D.L., Campbell, A.J., Prakapenka, V.B., Wanless, S.T., 2008. Melting and thermal expansion in the Fe–FeO system at high pressure. Earth Planet. Sci. Lett. 265, 655–665.

Sha, X.W., Cohen, R.E., 2010. First-principles thermal equation of state and thermoelasticity of hcp Fe at high pressures. Phys. Rev. B 81, 10.

Sharma, S.K., Sharma, B.K., 2010. Volume dependence of thermal expansivity for hcp iron. Phys. B Condes. Matter 405, 3145–3148.

Shen, G., Sturhahn, W., Alp, E.E., Zhao, J., Toellner, T.S., Prakapenka, V.B., Meng, Y., Mao, H.R., 2004. Phonon density of states in iron at high pressures and high temperatures. Phys. Chem. Miner. 31, 353–359.

Shen, G., Mao, H.K., Hemley, R.J., Duffy, T.S., Rivers, M.L., 1998. Melting and crystal structure of iron at high pressures and temperatures. Geophys. Res. Lett. 25, 373–376.

Simon, F., Glatzel, G., 1929. Remarks on fusion pressure curve. Z. Anorg. Allg. Chem. 178, 309–316.

Stacey, F.D., Davis, P.M., 2004. High pressure equations of state with applications to the lower mantle and core. Phys. Earth Planet. Inter. 142, 137–184.

Stixrude, L., Wasserman, E., Cohen, R.E., 1997. Composition and temperature of Earth's inner core. J. Geophys. Res. Solid Earth 102, 24729–24739.

Sturhahn, W., 2000. CONUSS and PHOENIX: evaluation of nuclear resonant scattering data. Hyperfine Interact. 125, 149–172.

Sturhahn, W., 2004. Nuclear resonant spectroscopy. J. Phys. Condes. Matter 16, S497–S530.

Sturhahn, W., Jackson, J.M., 2007. Geophysical applications of nuclear resonant spectroscopy. Geol. Soc. Am. Special Paper 421, 157–174.

Tateno, S., Hirose, K., Ohishi, Y., Tatsumi, Y., 2010. The structure of iron in Earth's inner core. Science 330, 359–361.

Vočadlo, L., Brodholt, J., Alfè, D., Gillan, M.J., Price, G.D., 2000. Ab initio free energy calculations on the polymorphs of iron at core conditions. Phys. Earth Planet. Inter. 117, 123–137.

Wasserman, E., Stixrude, L., Cohen, R.E., 1996. Thermal properties of iron at high pressures and temperatures. Phys. Rev. B 53, 8296–8309.

Williams, Q., Jeanloz, R., Bass, J., Svendsen, B., Ahrens, T.J., 1987. The melting curve of Iron to 250 Gigapascals: a constraint on the temperature at Earth's center. Science 236, 181–182.

Wojdyr, M., 2010. Fityk: a general-purpose peak fitting program. J. Appl. Crystallogr. 43, 1126–1128.